

# Selective Synthesis of 3D Aligned VO<sub>2</sub> and V<sub>2</sub>O<sub>5</sub> Carbon Nanotube Hybrid Materials by Chemical Vapor Deposition

Inga Dönges,<sup>[a]</sup> Sandeep Yadav,<sup>[a]</sup> Vanessa Trouillet,<sup>[b]</sup> and Jörg J. Schneider<sup>\*[a]</sup>

3D carbon nanotube hybrid materials containing VO<sub>2</sub> and V<sub>2</sub>O<sub>5</sub> evenly distributed onto vertically aligned carbon nanotubes (VACNTs) is reported. Adjustable loading of particles in controllable sizes and shapes onto the VACNTs was developed via a stepwise chemical vapour deposition (CVD) approach. Solid VO(acac)<sub>2</sub> is chosen as vanadium source. CO<sub>2</sub> acts as reactive gas for the pre-functionalisation of the VACNTs. The process temperature was identified as key parameter to control the deposited vanadium oxide phase. A temperature of 550 °C results in monoclinic VO<sub>2</sub>, while 600 °C results in the deposition of V<sub>2</sub>O<sub>5</sub> onto the VACNT support. The morphology and the

amount of deposited material was found to be dependent on the reactor dimensions and the degree of functionalisation of the carbon support. An increase of the D/G ratio of the VACNT from 0.75 to 1.08 caused by a CO<sub>2</sub> treatment step within the process led to an increase of the particle coverage from a scarce coverage without prior CO<sub>2</sub> treatment to a dense coverage of the VACNT support after 15 min of CO<sub>2</sub> exposure time. Size and crystallinity of the as deposited particles can be further adjusted by a controlled heat treatment after VO(acac)<sub>2</sub> precursor deposition.

## Introduction

The phase diagram of vanadium oxide contains different oxidic phases such as V<sub>2</sub>O<sub>5</sub>, VO<sub>2</sub>, V<sub>2</sub>O<sub>3</sub> and V<sub>6</sub>O<sub>13</sub> which differ in oxidation state and properties.<sup>[1]</sup> Monoclinic VO<sub>2</sub> for example is of special interest due to its metal-insulator transition at 68 °C.<sup>[2]</sup> This transition is caused by a change in the lattice of VO<sub>2</sub> from monoclinic structure to a metallic rutile VO<sub>2</sub> structure and is accompanied by a change in optical and electrical properties such as infrared reflectance and resistivity.<sup>[3]</sup> The relatively low switching temperature of 68 °C beholds potential for several applications such as temperature sensors,<sup>[4]</sup> memory<sup>[5]</sup> or switching devices<sup>[6]</sup> as well as thermochromic smart windows<sup>[7]</sup> in which VO<sub>2</sub> has been explored. Furthermore, VO<sub>2</sub> has been reported as gas sensing<sup>[8]</sup> and super capacitor material.<sup>[9]</sup> V<sub>2</sub>O<sub>5</sub> on the other hand is the thermodynamically most stable form of all known vanadium oxides<sup>[11]</sup> and has found applications in gas sensing,<sup>[10]</sup> super capacitors<sup>[11]</sup> and junction diodes.<sup>[12]</sup> Moreover, due to the variability in oxidation states vanadium oxide is also reported either as cathode<sup>[14]</sup> or anode<sup>[13]</sup> material in rechargeable batteries. Access to these oxides seems manifold and ranges from sol-gel,<sup>[15]</sup> hydrothermal<sup>[6]</sup> and CVD<sup>[16]</sup> routes to

ALD<sup>[17]</sup> and even more specialized ones.<sup>[18–20]</sup> All these methods result in a broad range of nanoscopic oxides in different shapes ranging from spherical particles,<sup>[21]</sup> coral type structures<sup>[22]</sup> to oxidic sheets<sup>[23]</sup> and needle like morphologies.<sup>[22]</sup> Binary composite materials with oxides (WO<sub>3</sub>,<sup>[24]</sup> TiO<sub>2</sub><sup>[25]</sup>) or carbon materials like CNTs,<sup>[26–28]</sup> graphene<sup>[29]</sup> or polymers<sup>[30]</sup> are reported to further increase the potential application for vanadium oxides. Especially the combination of VO<sub>x</sub> and CNTs has sparked interest and has been widely explored and often shows enhanced performance in comparison to pristine vanadium oxides, like in Mott devices, where it is described that the addition of CNTs significantly increases the spiking frequency compared to a device where VO<sub>2</sub> only as sole component is employed.<sup>[33]</sup> Synthesis of VO<sub>x</sub>@CNT composites can be obtained by gas phase routes which are often reported to be demanding within their routine. A VO<sub>x</sub> coating onto spatially ordered CNT by ALD, results in the deposition of poorly crystalline V<sub>2</sub>O<sub>5</sub>, which needs additional post treatment to form the desired crystalline VO<sub>2</sub>@CNT material.<sup>[34]</sup> In contrast, a CVD process, which aims for a direct deposition of V<sub>2</sub>O<sub>5</sub> results in a superficial coating mainly on the surface of the CNT array and is accompanied by a loss of the array structure due to oxidation of the CNTs at the necessary high process temperature of 900 °C. To the best of our knowledge the reported gas phase routes to VO<sub>x</sub>@VACNT offer the possibility to investigate such composite materials for the first time with respect to a defined control of designated particle shape and size. With this work we report on a facile method with a broad range of control on the resulting hybrid VO<sub>x</sub>@VACNT materials. This is achieved by using a well-defined precursor molecule, VO(acac)<sub>2</sub> and CO<sub>2</sub> as reactive gas component. The usage of CO<sub>2</sub> is twofold. On the one hand it serves as reactive component for the deposition of the oxide species from the molecular vanadium precursor and allows to control the oxygen supply by controlling the reaction temperature. On the other hand it allows a pre-treatment of the

[a] I. Dönges, S. Yadav, J. J. Schneider

Fachbereich Chemie, Eduard-Zintl-Institut für Anorganische und Physikalische Chemie, Technische Universität Darmstadt, Peter-Grünberg-Str. 12, 64287 Darmstadt, (Germany)  
E-mail: joerg.schneider@tu-darmstadt.de

[b] V. Trouillet

Institute for Applied Materials (IAM-ESS) and Karlsruhe Nano Micro Facility (KNMF), Karlsruhe Institute of Technology (KIT), Hermann-von-Helmholtz-Platz 1, 76344 Eggenstein-Leopoldshafen (Germany)

© 2024 The Author(s). Chemistry - A European Journal published by Wiley-VCH GmbH. This is an open access article under the terms of the Creative Commons Attribution Non-Commercial License, which permits use, distribution and reproduction in any medium, provided the original work is properly cited and is not used for commercial purposes.

CNTs within the 3D VACNT array. Here the  $\text{CO}_2$  acts as a functionalising reactive molecule which introduces reactive anchoring sites on the CNT surface by selective oxidation. Together with an understanding of the impact of crucial experimental parameters like temperature and geometric reactor constraints this work aims for a controlled gas phase approach to  $\text{VO}_x$ @VACNT composites. It thus allows the creation of a routine in which the control of oxide coating on the interior and exterior surface area of the 3D VACNT array is possible. In addition, particle size, shape, crystallinity and density of the deposits is adjustable. Finally, the overall process demonstrates a highly flexible synthesis method, which offers future possibilities for further exploration into the gas phase synthesis of other 3D arranged nano composite materials.

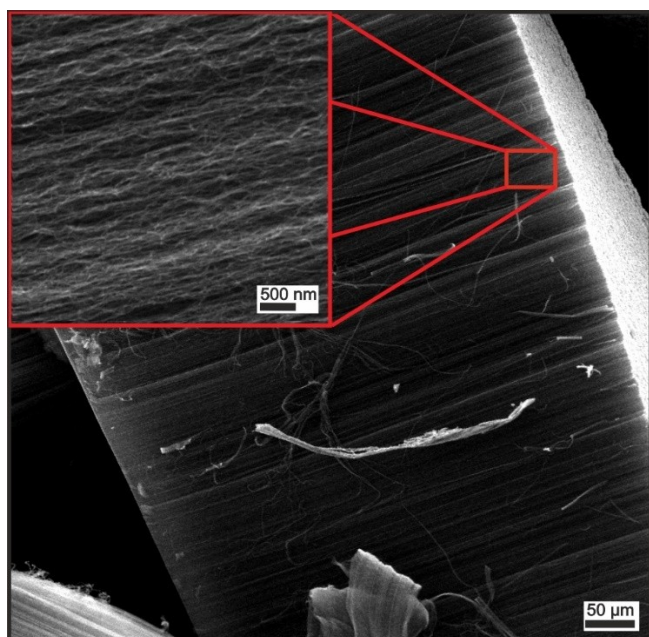


Figure 1. SEM Images of the VACNTs at different magnifications.

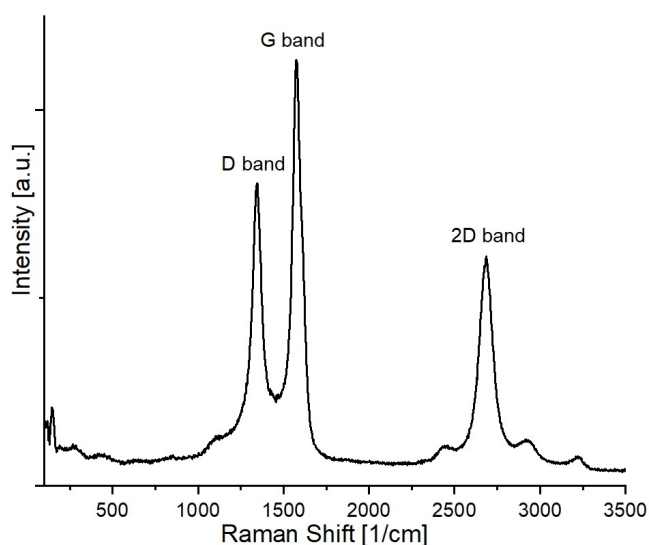


Figure 2. Raman spectrum of the synthesised VACNT.

## Results and Discussion

### Characterisation of the VACNT Substrate

SEM images of the as-prepared VACNT (Figure 1) show the vertical alignment of the CNT with a height of  $\sim 500 \mu\text{m}$ .

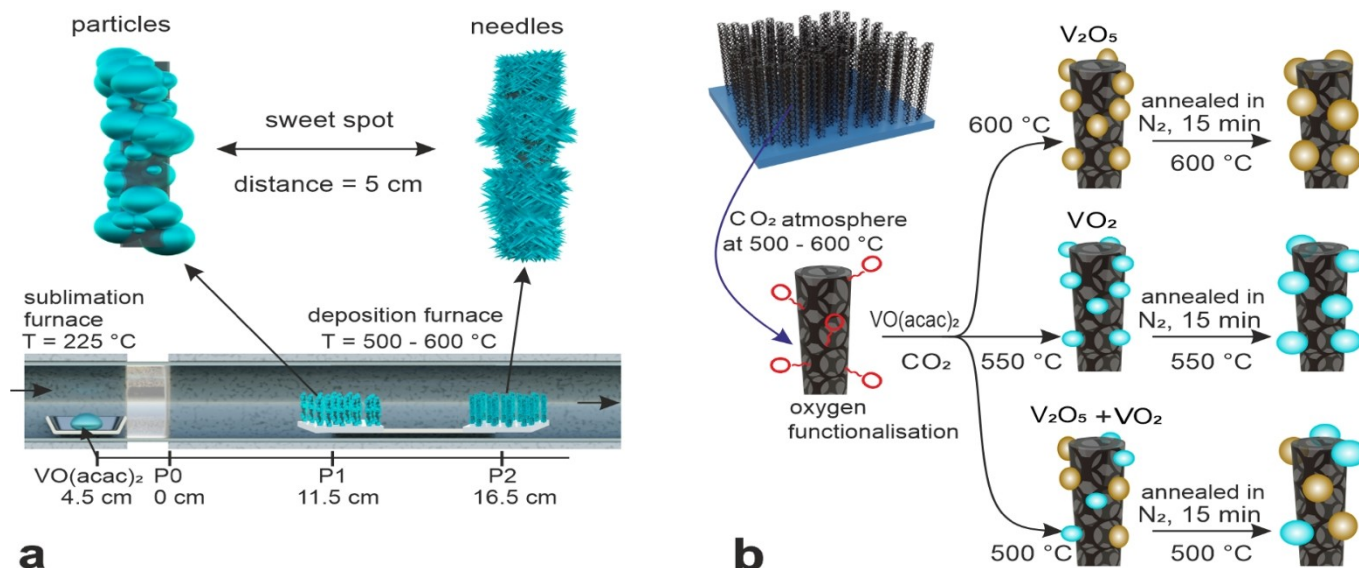
The Raman spectra (Figure 2) of the VACNT show the characteristic D-band at  $1345 \text{ cm}^{-1}$  mainly indicative for defects, surface and edge functionalisation and amorphous carbon contamination. The G-band at  $1575 \text{ cm}^{-1}$  is related to the graphitic  $\text{sp}^2$  framework structure. The ratio of  $\text{sp}^3$  carbon to  $\text{sp}^2$  carbon is an important quality indicator. A ratio below 1 is favourable and the herein employed VACNTs show an average ratio of 0.75.

### Synthesis and Characterization of $\text{VO}_2$ @VACNT and $\text{V}_2\text{O}_5$ @VACNT Composite Structures

A systematic study of the influence of various process parameters like (i) synthesis temperature, (ii) surface functionalisation of the VACNT host structure and (iii) post annealing on the deposited vanadium oxide particles on the surface of the VACNT arrays was performed. Especially the formation of oxide phases, changes of morphology and deposition density of vanadium oxide is of great interest. Scheme 1 illustrates the reaction and the different synthesis conditions employed.

$\text{VO}(\text{acac})_2$  precursor solutions are often reported to be employed for the deposition of vanadium oxides in CVD processes.<sup>[21,22,36]</sup> However, these solutions are reported to show a remarkable aging effect with time, which is experimentally hard to control and therefore needs stringent parameters to be followed resulting in a significant influence on the deposited oxide particles or films.<sup>[22]</sup> In contrast, solid  $\text{VO}(\text{acac})_2$  as precursor allows a more stable and continuous process, in exchange for a close temperature and pressure control during sublimation. Optimum conditions were observed within a narrow temperature window of  $200^\circ\text{C}$  to max.  $250^\circ\text{C}$ . These temperatures are allowing a controllable sublimation without precursor decomposition. Similar to the precursor sublimation, the synthesis process temperature must be chosen carefully. The formation of different vanadium oxide phases is reported within the employed temperatures of  $500^\circ\text{C}$  to  $600^\circ\text{C}$ .<sup>[11]</sup> Accordingly, XRD spectra of samples synthesised at  $500^\circ\text{C}$  (Figure 3, green trace) show reflexes assigned to  $\text{VO}_2$  and  $\text{V}_2\text{O}_5$  alongside each other. An increased process temperature of  $600^\circ\text{C}$  causes the sole deposition of  $\text{V}_2\text{O}_5$  according to XRD (Figure 3 yellow trace). At  $550^\circ\text{C}$  all signals within the resulting XRD could be assigned to the monoclinic  $\text{VO}_2$  pattern (Figure 3 petrol trace).

Figure 4a shows the XPS survey spectra of the  $\text{VO}_x$ @VACNT sample prepared at  $600^\circ\text{C}$ , where C, O, and V are detected, while no other elements were found. The C 1s core spectra of the  $\text{VO}_x$ @VACNT samples (Figure 4b) show one main signal at a binding energy of 284.4 eV corresponding to  $\text{sp}^2$  graphitic carbon and three further peaks with very weak intensity at 285.0, 286.4 and 288.7 eV corresponding to C–C, C–H  $\text{sp}^3$



**Scheme 1.** Schematic of the experimental set-up and its influence on the obtained sample morphology (a) while b shows a schematic of the experimental procedure together with an outcome of the various phases depending on reaction conditions.

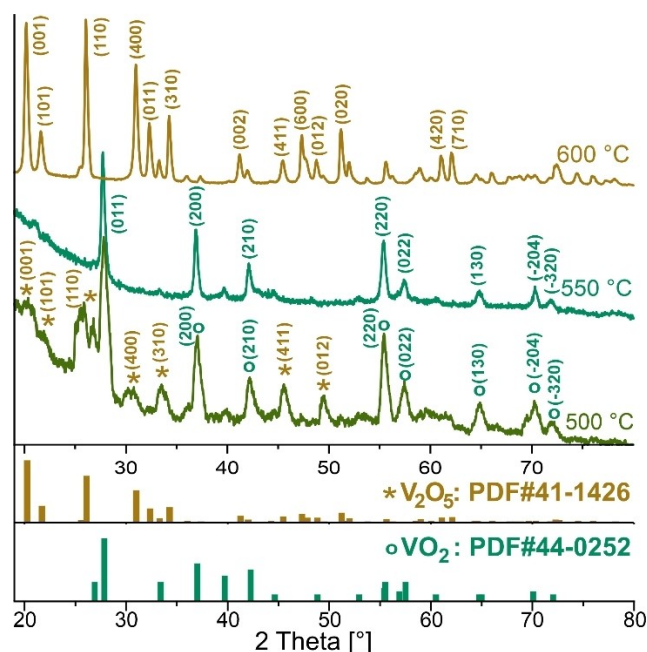


**Figure 3.** XRD pattern of samples deposited at temperatures of 500, 550 and 600 °C with the respective lattice planes indexed according to the JCPDS reference data.

hybridised carbon, C–O and O=C=O species respectively, which are in accordance with binding energies of carbon moieties in VACNT structures.<sup>[46]</sup> The corresponding O 1s core spectra (Figure 4c) depicts three signals at binding energies of 530.3, 531.2 and 533.1 eV. The first and most intensive peak can be assigned to oxygen bound to vanadium, whereas the two further ones can be ascribed to C=O and C–O respectively.<sup>[46]</sup> For V 2p<sub>3/2</sub> (Figure 4c), binding energies of 515.7 and 517.4 eV for V<sup>4+</sup> and V<sup>5+</sup> are observed and are in good agreement with values reported in literature.<sup>[42,43]</sup> The surface states of vanadium

oxide has been subject to various studies,<sup>[47,48]</sup> where it has been shown, that V<sup>4+</sup> in VO<sub>2</sub> is prone towards extensive oxidation even under ambient conditions. According to a quantitative estimation for the sample synthesized at 550 °C, ~30% of V<sup>4+</sup> on the surface of VO<sub>2</sub> particles is oxidatively converted into V<sup>5+</sup>. This is indeed in good agreement to earlier studies on VO<sub>2</sub> prepared by CVD.<sup>[44]</sup> Interestingly V–K-edge-XANES studies have convincingly shown that despite a significant surface oxidation to V<sub>2</sub>O<sub>5</sub> the bulk of such samples remains still VO<sub>2</sub>.<sup>[44]</sup> This matches our findings for the VO<sub>2</sub>@VACNT material. Therefore, formation of a VO<sub>2</sub>/V<sub>2</sub>O<sub>5</sub> VO<sub>2</sub>/V<sub>2</sub>O<sub>5</sub> core shell particle due to this partial surface oxidation is a reasonable explanation.

The V<sub>2</sub>O<sub>5</sub>@VACNT composite sample synthesized at 600 °C, the V 2p doublets could be assigned to the two vanadium species V<sup>4+</sup> (V 2p<sub>3/2</sub> at 516.0 eV) and V<sup>5+</sup> (V 2p<sub>3/2</sub> at 517.5 eV), the latter representing the main vanadium species. The presence of V<sup>4+</sup> within this sample can be explained due to the carbothermic reaction between the V<sup>5+</sup> and the all carbon VACNT substrate which partially reduces the formed V<sub>2</sub>O<sub>5</sub>.<sup>[45,46]</sup> This fact is responsible for the missing VO<sub>2</sub> diffraction peaks in the XRD. At the lowest process temperature of 500 °C, the V<sub>2</sub>O<sub>5</sub> formation on VACNTs is more pronounced than in the sample prepared at 550 °C. A quantitative determination shows that ~83% of the V 2p<sub>3/2</sub> signal can be assigned to V<sup>5+</sup> compared to only ~30% calculated for the 550 °C sample. Studies on the VO(acac)<sub>2</sub> precursor have shown, that at 500 °C the formation of vanadium oxide is dependent on the additional oxygen flow, while at 550 °C it is not. For intermediate oxygen flows, comparable to the herein applied CO<sub>2</sub> stream, the formation of a mixed V<sup>4+</sup>/V<sup>5+</sup> species is reported.<sup>[49]</sup> In summary the combined XPS results confirm the XRD results and thus show, that the individual phase formation of vanadium oxides is strongly dependent on the process temperature.

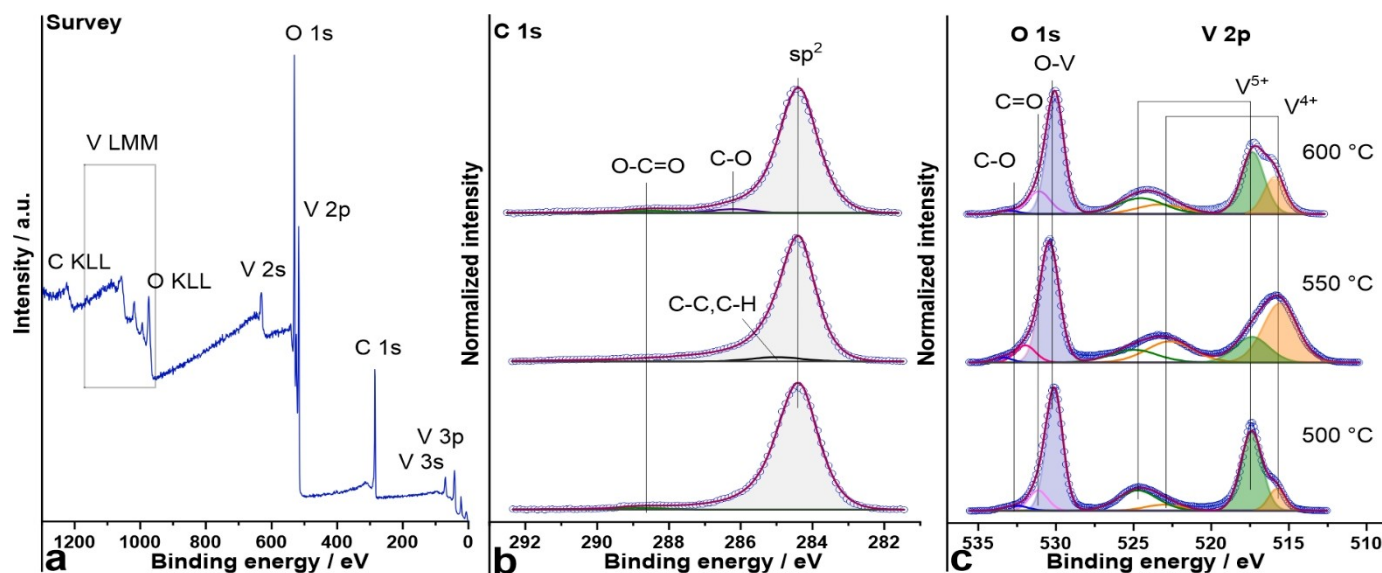


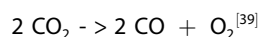
**Figure 4.** a) XPS survey spectrum of a VO<sub>x</sub>@VACNT sample synthesized at 600 °C. b) and c), show the C 1s, O 1s and V 2p core spectra of VO<sub>x</sub>@VACNT sample prepared at 500 °C, 550 °C, 600 °C.

Within the individual given reactor geometry (see experimental section) a “sweet spot” zone with a length of 5 cm could be determined, where even a control on the morphology of the deposited vanadium oxide polymorph is possible. Deposition onto the substrate placed at the start of the sweet spot zone results in particles that are equally round and spherically shaped (Figure 5a, c and e). Deposition onto

substrates placed at the end of the sweet spot zone however yields a needle like morphology of the deposited VO<sub>2</sub> (Figure 5b, d and f). By inspection of the TEM images (Figure 5e and f) a conformation of the deposition of the different morphologies achieved by the different positioning in the reactor becomes visible.

Another important parameter in the controlled synthesis of the vanadium oxide/VACNT hybrid material is the influence of the process gas CO<sub>2</sub> on the substrate as well as on the deposition process. Figure 6 shows the normalised Raman spectra of VACNTs before and after a treatment step of 15 min where it is evident that the CO<sub>2</sub> treatment causes an increase in the D-band and a decrease in the intensity of the G-band, which results in a change of the D/G ratio from 0.75 to 1.08. This ratio change can be understood as an increase of structural defects in the CNT structure due to the oxidising conditions introduced by the CO<sub>2</sub> gas treatment.

These defects have been created due to the reaction between the CNT and the oxygen which is generated from the thermal decomposition of CO<sub>2</sub> at temperatures of 500 °C and higher according to the following equation.



The CO<sub>2</sub> disproportionation reaction thus presents an important functionalisation process which generates oxygen in situ. It allows to prepare the VACNT surface for a controlled tethering of the reactive precursor fragments generated from the vanadium oxide precursor VO(acac)<sub>2</sub>. Additionally CO<sub>2</sub> is most helpful in the process since it operates as an oxidising component needed to prevent a reduction of V<sup>4+</sup> by CO and H<sub>2</sub> which are decomposition products of VO(acac)<sub>2</sub>.<sup>[40]</sup> Different CO<sub>2</sub> conditioning times in a time range between 0 to 30 min have been investigated. Longer CO<sub>2</sub> treatment times result in a denser particle coverage of the CNT surface. If no CO<sub>2</sub> treatment

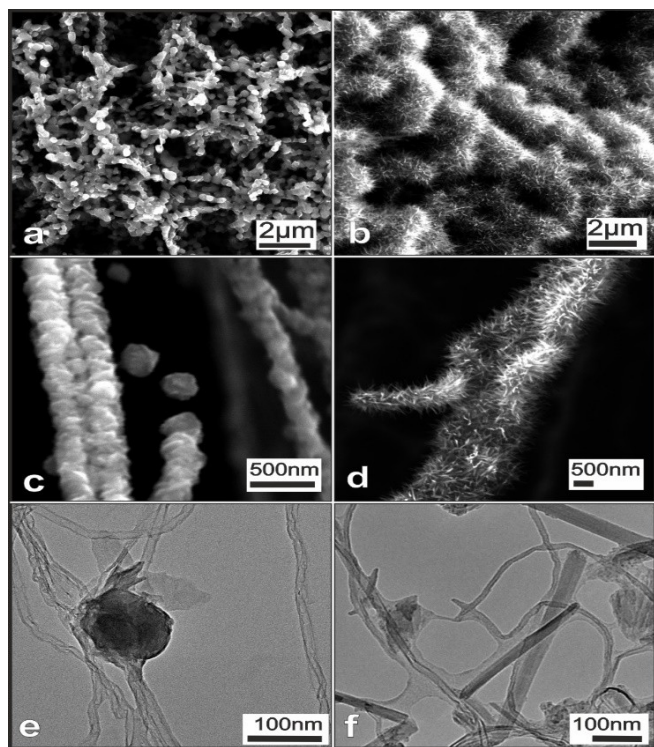


**Figure 5.** SEM and TEM images of the resulting morphologies of the VO<sub>2</sub> polymorphs observed depending on the substrate positioning within the “sweet spot” reactor area at different magnifications.

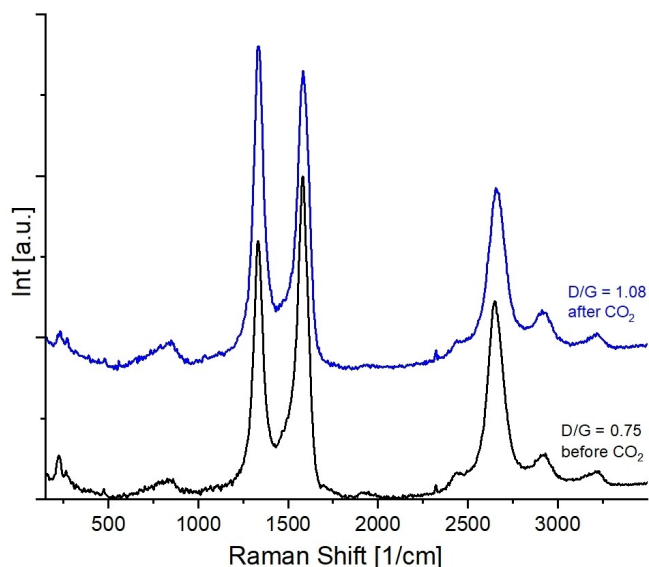


**Figure 6.** Raman spectra of VACNTs before (black trace) and after (blue trace)  $\text{CO}_2$  treatment.

prior to the particle deposition has been done a rather scarce coverage with only a shattered particle deposition is observable within the VACNT array (Figure 7a, c and e).

In comparison samples which have been pre-treated with  $\text{CO}_2$  show a rather dense tethering of individual and intergrown particles within the VACNT array (Figure 7b, d and f).

Indeed, this increase in oxide coverage is substantiated by a gravimetric increase as followed by a thermogravimetric analysis of the remaining vanadium oxide phase after thermal elimination of the VACNT substrate matrix. A thermogravimetric measurement of a composite sample of same size treated for 15 min with  $\text{CO}_2$  shows a residual mass of 34 weight %, while only 28% residual mass is obtained from a sample without any  $\text{CO}_2$  functionalisation. Longer  $\text{CO}_2$  treatment times of 30 min did not result in a denser coverage of the inner tube surface indicating that surface functionalisation/activation might have reached a certain culmination point for the given sample size.

Besides an obviously denser coverage the amount of deposited particles within the array has no structural impact on the resulting hybrid material deposited (morphology, crystallinity). Optimising the reaction conditions with these findings, a time of five min  $\text{CO}_2$  treatment was found as sufficient to achieve a dense coverage inside the VACNT array without depositing an additional amount of oxide on the external outer surface

### Effect of Annealing on Oxide Crystallinity

To study the impact of an additional temperature treatment on the particle crystallinity and size, the vanadium oxide decorated VACNTs were kept at the individual process temperatures in a nitrogen stream for different time intervals right after the initial deposition was finished. This leads to an increase in size of the deposited particles. Samples, which were annealed for 15 min,

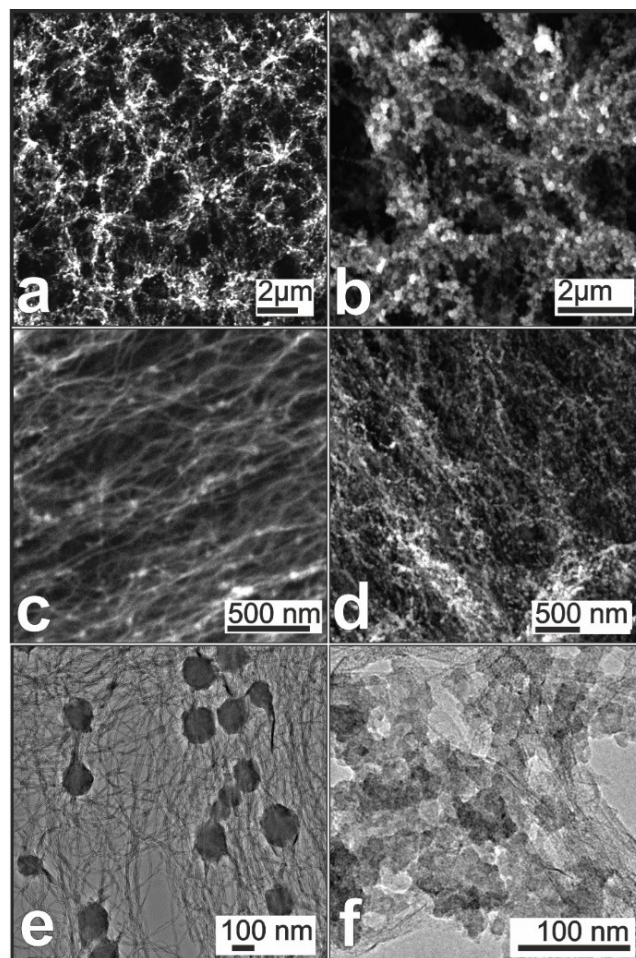


**Figure 7.** SEM and TEM images of samples with zero (a, c, e) and 15 min (b, d, f)  $\text{CO}_2$  pre-conditioning time under different magnifications. A and b show a top view; b and d a view inside the VACNT arrays obtained by mechanical opening of the structure. TEM images are obtained by unHINGING the VACNT structure with ultrasonication.

showed a significant particle increase up to 170 nm compared to particles without annealing which show an average size of 70 nm as displayed in Figure 8. Typically, an Ostwald ripening process accounts for this observation, due to a significant decrease in particle numbers compared to samples which are not processed further.

Apart from the influence on the particle size the additional thermal processing also enables an improvement of the crystallinity of the deposited vanadium oxide. Figure 9 (green trace) shows the XRD and Raman spectrum of a sample which has been subject to 15 min annealing. As a comparison XRD and Raman spectra of a sample without annealing (Figure 9 black trace) reveal an amorphous nature of the deposited particles.

Interestingly, in the formed  $\text{VO}_2/\text{VACNT}$  composite the deposited  $\text{VO}_2$  is still reactive to reduction. When changing the gas conditions after the initial synthesis and flowing diluted hydrogen gas ( $\text{H}_2/\text{N}_2$  1:10) at  $550^\circ\text{C}$  the sample obtains a metallic shimmering glow probably indicating formation of a sub stoichiometric, amorphous vanadium oxide bronze materi-

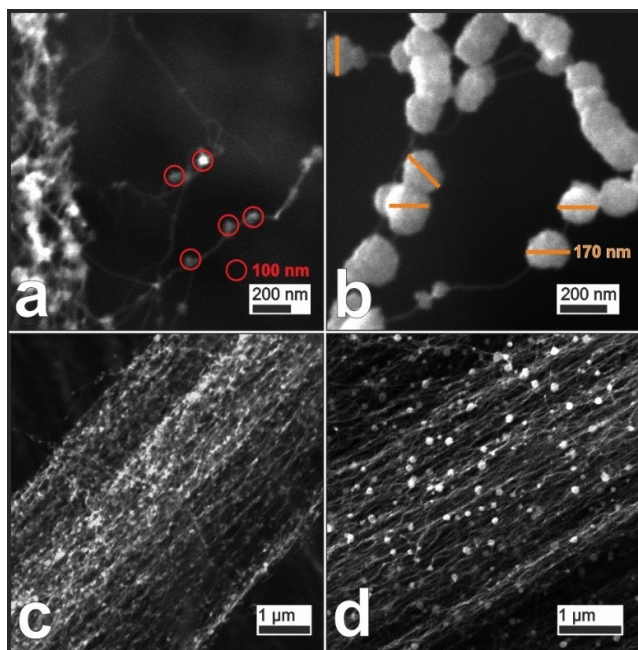


**Figure 8.** SEM images of composite samples with no (a, c) and 15 min (b, d) formation, holding time under initial synthesis temperature conditions.

al, well known for vanadium with its ability to stabilize mixed valency states in an oxidic environment. Indeed, a high vanadium content detected by EDS (89%) supports this suggestion. Furthermore, the obtained XRD (Figure 9c) of this vanadium oxide bronze material shows a cubic phase diffraction pattern.

## Conclusions

A gas phase CVD access to the controlled synthesis of different morphologies as well as particle loadings, particle sizes and crystallinity of  $\text{VO}_2$  and  $\text{V}_2\text{O}_5$  nanoparticles is presented. These oxides can be selectively deposited and tethered on the inner and outer surface and of three-dimensionally organized

VACNTs. The parameters which control the deposition and formation of the  $\text{VO}_2$ @VACNT and  $\text{V}_2\text{O}_5$ @VACNT composites are studied systematically. Due to the controllable deposition the outer surface of the 3D VACNT block structure experiences no clogging with surplus oxide deposition, which is often the case when an uncontrolled deposition is performed. The density of deposited  $\text{VO}_2$  oxide particles can be steered by oxygen functionalisation with  $\text{CO}_2$  which increases the number of defects on the surface as detected by Raman spectroscopy. By further annealing under the same reaction temperature Ostwald ripening of the as synthesized  $\text{VO}_2$  particles can be observed and leads to controllable particle sizes. Using sweet spot conditions in the reactor zone the formation of different morphologies either particles or needles is achievable. The developed method sheds light on the importance of controlling experimental parameters for obtained well defined phases and morphologies of metal oxides as exemplified herein for the case of vanadium oxides. It can be speculated that a similar approach might lead to a control of different phases for other oxides on other carriers too.

## Experimental Section

### Growth of Vertically Aligned CNTs (VACNTs)

VACNTs were synthesized by a water assisted chemical vapour deposition (WACVD). On a  $1.5\text{ cm} \times 1.5\text{ cm}$  Si/SiO<sub>2</sub> wafer 12–15 nm Al was thermally deposited followed by a layer of 1.6–1.8 nm of Fe deposited by plasma sputtering. The VACNTs were grown in a tube furnace using ethylene (200 sccm) as carbon source on this wafer at  $T = 850^\circ\text{C}$  for a duration of 10 min. A small amount of water (~550 ppm) was used to enhance the quality of the CNT. The resulting CNTs are multiwalled (4–6 walls) with a height of approx.  $500\ \mu\text{m}$ .<sup>[35]</sup>

### Synthesis of the $\text{VO}_x$ @CNTs using CVD

Deposition of the vanadium oxide particles was done by chemical vapour deposition in a three-zone tube furnace. Solid  $\text{VO}(\text{acac})_2$  was used as a precursor and placed in glass boat 4.5 cm in front of the furnace in a separate small furnace. The VACNT sample was

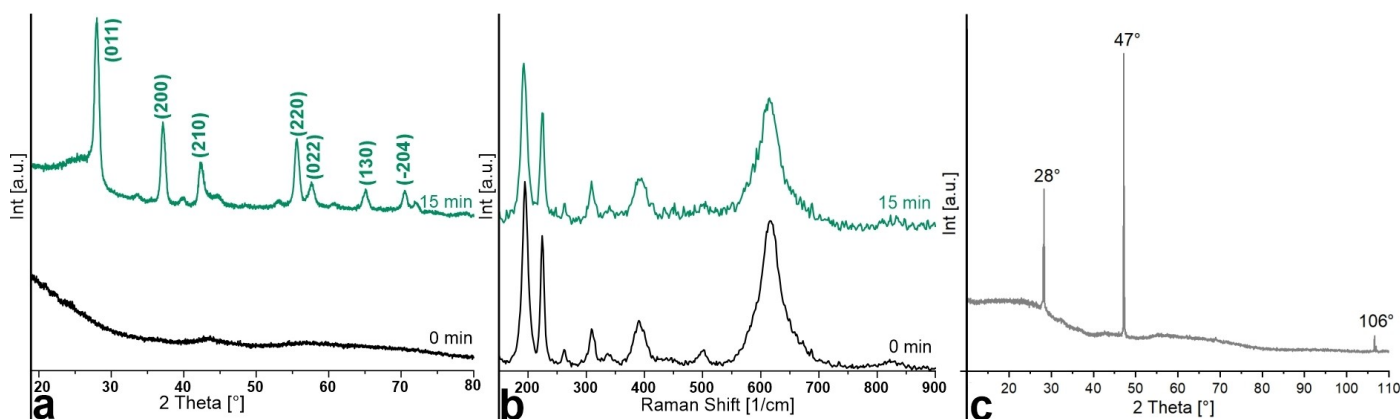


**Figure 9.** XRD (a) and Raman (b) spectra of samples without (black trace) and after 15 min (green trace) annealing, holding time under initial temperature conditions. c) is an XRD pattern of the reduced vanadium rich  $\text{V}_x\text{O}_y$  phases.

placed in a four cm diameter quartz-tube 11.5 to 16.5 cm into the furnace (See Figure 3b) and flushed for 30 min with 500 sccm N<sub>2</sub> to ensure a nitrogen atmosphere. Afterwards the flow was reduced to 200 sccm N<sub>2</sub> and the furnace was heated to process temperatures between 500 and 600 °C, (see main text). 20 sccm of CO<sub>2</sub> were added to the gas stream for further functionalisation of the VACNT for a varying amount of time (typically 5 min, see main text). Afterwards, deposition of the precursor was started by heating the second furnace to 225 °C. After 10 min of deposition the sublimation furnace was turned off and the CO<sub>2</sub> flow was stopped. The sample was kept for up to 15 min at a N<sub>2</sub> flow of 200 sccm and a defined process temperature of 550 °C (see main text). Thereafter the reactor was cooled down to room temperature under laminar N<sub>2</sub> flow.

### Materials Characterisation

XRD was recorded measured on a Rigaku Miniflex 600@40 kV 15 mA diffractometer using Cu K $\alpha$  radiation ( $\lambda=1.541 \text{ \AA}$ ). Scanning electron microscopy were performed on a Philips XL-30 FEG. Transmission electron microscopy was performed on a Tecnai G2 F20 microscope operating at 200 kV. TEM samples were prepared by drop casting a dispersion of the nanocomposite in ethanol obtained by ultrasonication onto a TEM copper grid. Thermogravimetric measurements were performed on a Netzsch 209 F1. The sample was measured in an aluminium oxide crucible and heated with a rate of 5 K/min to 750 °C in an oxygen atmosphere. Raman measurements were performed on a ThermoScientific DXR3 Raman Microscope employing a 532 nm laser with a high-resolution grading. XPS measurements were performed using a K-Alpha+ XPS spectrometer (ThermoFisher Scientific). The Thermo Avantage software was used for data acquisition and processing. All samples were analysed using a microfocused, monochromated Al K $\alpha$  X-ray source (400  $\mu\text{m}$  spot size). The K-Alpha+ charge compensation system was employed during analysis, using electrons of 8 eV energy, and low-energy argon ions to prevent any localized charge build-up. The spectra were fitted with one or more Voigt profiles (BE uncertainty:  $\pm 0.2 \text{ eV}$ ) and Scofield sensitivity factors were applied for quantification.<sup>[41]</sup> All spectra were referenced to the C 1s peak (C–C, C–H) at 285.0 eV binding energy controlled by means of the well-known photoelectron peaks of metallic Cu, Ag, and Au, respectively.

### Acknowledgements

TEM measurements were done at the ERC Jülich, Germany under contract ERC-TUDa. We thank Jörg Engstler (TEM) and Silvio Heinschke (XRD) both at TUDa for measurements. ID likes to thank T. Böttcher for providing the 3 D graphics. Open Access funding enabled and organized by Projekt DEAL.

### Conflict of Interests

The authors declare no conflict of interest.

### Data Availability Statement

The data that support the findings of this study are available from the corresponding author upon reasonable request.

**Keywords:** Carbon nanotubes · CVD · Gas phase · Oxide composites · Vanadium oxide

- [1] P. Hu, P. Hu, T. D. Vu, M. Li, S. Wang, Y. Ke, X. Zeng, L. Mai, Y. Long, *Chem. Rev.* **2023**, *123*, 4353–4415.
- [2] J. H. Park, J. M. Coy, T. S. Kasirga, C. Huang, Z. Fei, S. Hunter, D. H. Cobden, *Nature* **2013**, *500*, 431–434.
- [3] F. J. Morin, *Phys. Rev. Lett.* **1959**, *3*, 34–36.
- [4] B.-J. Kim, Y. W. Lee, B.-G. Chae, S. J. Yun, S.-Y. Oh, H.-T. Kim, Y.-S. Lim, *Appl. Phys. Lett.* **2007**, *90*, 023515.
- [5] E. Corti, A. Khanna, K. Niang, J. Robertson, K. E. Moselund, B. Gotsmann, S. Datta, S. Karg, *IEEE Electron Device Lett.* **2020**, *41*, 629–632.
- [6] S. Bae, S. Lee, H. Koo, L. Lin, B. H. Jo, C. Park, Z. L. Wang, *Adv. Mater.* **2013**, *25*, 5098–5103.
- [7] L. Long, H. Ye, *Sci. Rep.* **2014**, *4*, 6427.
- [8] R. Basu, P. R. Reshma, A. K. Prasad, S. Dhara, *Mater. Chem. Phys.* **2020**, *248*, 122901.
- [9] P. H. Jampani, K. Kadakia, D. H. Hong, R. Epur, J. A. Poston, A. Manivannan, P. N. Kumta, *J. Electrochem. Soc.* **2013**, *160*, A1118–A1127.
- [10] V. Mounasamy, G. K. Mani, D. Ponnusamy, K. Tsuchiya, P. R. Reshma, A. K. Prasad, S. Madanagurusamy, *Anal. Chim. Acta* **2020**, *1106*, 148–160.
- [11] S. S. Karade, *J. Electroanal. Chem.* **2020**, *10*.
- [12] I. Pradeep, E. Ranjith Kumar, N. Suriyanarayanan, C. Srinivas, N. Venkata Rao, *J. Mater. Sci. Mater. Electron.* **2018**, *29*, 9840–9853.
- [13] B. Xiao, B. Zhang, J. Zheng, L. Tang, C. An, Z. He, H. Tong, W. Yu, *Ceram. Int.* **2018**, *44*, 13113–13121.
- [14] B. D. Boruah, B. Wen, M. De Volder, *Nano Lett.* **2021**, *21*, 3527–3532.
- [15] M. Gotić, S. Popović, M. Ivanda, S. Musić, *Mater. Lett.* **2003**, *57*, 3186–3192.
- [16] E. Koudoumas, K. T. Le, D. Vernardou, *Energy Nexus* **2023**, *11*, 100237.
- [17] M.-G. Willinger, G. Neri, A. Bonavita, G. Micali, E. Rauwel, T. Hertrich, N. Pinna, *Phys. Chem. Chem. Phys.* **2009**, *11*, 3615.
- [18] A. J. Santos, M. Escanciano, A. Suárez-Llorens, M. Pilar Yeste, F. M. Morales, *Chem. – Eur. J.* **2021**, *chem.202102566*.
- [19] I. Mjejri, A. Rougier, M. Gaudon, *Inorg. Chem.* **2017**, *56*, 1734–1741.
- [20] X. J. Wang, H. D. Li, Y. J. Fei, X. Wang, Y. Y. Xiong, Y. X. Nie, K. A. Feng, *Appl. Surf. Sci.* **2001**.
- [21] C. Piccirillo, R. Binions, I. P. Parkin, *Chem. Vap. Deposition* **2007**, *13*, 145–151.
- [22] Y.-T. Wang, C.-H. Chen, *Inorg. Chem.* **2013**, *52*, 2550–2555.
- [23] M. M. Rahman, J.-Z. Wang, N. H. Idris, Z. Chen, H. Liu, *Electrochim. Acta* **2010**, *56*, 693–699.
- [24] J.-H. Cho, Y.-J. Byun, J.-H. Kim, Y.-J. Lee, Y.-H. Jeong, M.-P. Chun, J.-H. Paik, T. H. Sung, *Ceram. Int.* **2012**, *38*, S589–S593.
- [25] P. H. Jampani, O. Velikokhatnyi, K. Kadakia, D. H. Hong, S. S. Damle, J. A. Poston, A. Manivannan, P. N. Kumta, *J. Mater. Chem. A* **2015**, *3*, 8413–8432.
- [26] N. Arya, D. Verma, V. Balakrishnan, *Nanotechnology* **2023**, *34*, 115401.
- [27] G. P. Evans, M. J. Powell, I. D. Johnson, D. P. Howard, D. Bauer, J. A. Darr, I. P. Parkin, *Sens. Actuators B Chem.* **2018**, *255*, 1119–1129.
- [28] K. S. Karimov, M. Mahroof-Tahir, M. Saleem, M. T. S. Chani, A. K. Niazi, *J. Semicond.* **2015**, *36*, 073004.
- [29] Y. Liu, Y. Zhang, T. Hu, Y. Mu, J. Sun, J. Zheng, H. Jiang, X. Dong, C. Meng, *Colloids Surf. Physicochem. Eng. Asp.* **2020**, *586*, 124222.
- [30] S. Kabir, D. Yang, A. B. Ahmad Kayani, H. Zhang, S. Nirantar, S. Sriram, S. Walia, M. Bhaskaran, *ACS Appl. Nano Mater.* **2022**, *5*, 10280–10291.
- [31] D. J. Babu, J. J. Schneider, *Chem. Ing. Tech.* **2017**, *89*, 1273–1287.
- [32] S. J. Paul, I. Sharma, I. Elizabeth, B. Gahtori, M. R. M. S. S. Titus, P. Chandra, B. K. Gupta, *ACS Appl. Mater. Interfaces* **2020**, *12*, 16946–16958.
- [33] S. M. Bohaichuk, S. Kumar, G. Pitner, C. J. McClellan, J. Jeong, M. G. Samant, H. S. P. Wong, S. S. P. Parkin, R. S. Williams, E. Pop, *Nano Lett.* **2019**, *19*, 6751–6755.
- [34] V. P. Prasad, F. V. Ramirez, I. Papakonstantinou, I. P. Parkin, N. Bahlawane, *ACS Appl. Nano Mater.* **2020**, *3*, 8848–8857.
- [35] R. Joshi, J. Engstler, L. Houben, M. Bar Sadan, A. Weidenkaff, P. Mandaliev, A. Issanin, J. J. Schneider, *ChemCatChem* **2010**, *2*, 1069–1073.
- [36] D. Vernardou, M. E. Pemble, D. W. Sheel, *Chem. Vap. Deposition* **2006**, *12*, 263–274.
- [37] R. N. Nenashev, N. E. Mordvinova, V. P. Zlomanov, V. L. Kuznetsov, *Inorg. Mater.* **2015**, *51*, 891–896.
- [38] Z. Zhang, Z. Wang, S. He, C. Wang, M. Jin, Y. Yin, *Chem. Sci.* **2015**, *6*, 5197–5203.
- [39] R. N. Nenashev, N. E. Mordvinova, V. P. Zlomanov, V. L. Kuznetsov, *Inorg. Mater.* **2015**, *51*, 891–896.

- [40] M. H. Lietzke, C. Mullins, *J. Inorg. Nucl. Chem.* **1981**, *43*, 1769–1771.
- [41] J. H. Scofield, *Phenomena* **1976**, *8*, 129–137.
- [42] G. Silversmit, D. Depla, H. Poelman, G. B. Marin, R. De Gryse, *J. Electron Spectrosc. Relat. Phenom.* **2004**, *135*, 167–175.
- [43] M. C. Biesinger, L. W. M. Lau, A. R. Gerson, R. S. C. Smart, *Appl. Surf. Sci.* **2010**, *257*, 887–898.
- [44] M. J. Powell, I. J. Godfrey, R. Quesada-Cabrera, D. Malarde, D. Teixeira, H. Emerich, R. G. Palgrave, C. J. Carmalt, I. P. Parkin, G. Sankar, *J. Phys. Chem. C* **2017**, *121*, 20345–20352.
- [45] K. A. Juggernaut, M. Kim, K. Kim, J. Li, A. A. McLane, J. Lee, A. J. Hart, J. G. Ok, *Ceram. Int.* **2021**, *47*, 32342–32348.
- [46] G. Sun, H. Ren, Z. Shi, L. Zhang, Z. Wang, K. Zhan, Y. Yan, J. Yang, B. Zhao, *J. Colloid Interface Sci.* **2021**, *588*, 847–856.
- [47] J. Mendialdua, R. Casanova, Y. Barbaux, *J. Electron Spectrosc. Relat. Phenom.* **1995**, *71*, 249–261.
- [48] G. Silversmit, H. Poelman, D. Depla, N. Barrett, G. B. Marin, R. De Gryse, *Surf. Interface Anal.* **2006**, *38*, 1257–1265.
- [49] D. Vernardou, M. E. Pemble, D. W. Sheel, *Chem. Vap. Deposition* **2006**, *12*, 263–274.

---

Manuscript received: May 23, 2024

Accepted manuscript online: September 12, 2024

Version of record online: October 29, 2024